Pergamon

Int. J. Heat Mass Transfer. Vol. 37, No. 10, pp. 1433–1440, 1994

0017-9310/94 $7.00+0.00

0017-9310(93)E0101-L

Knudsen void gas heat transport in fibrous media

LEI ZHENG and WILLIAM STRIEDER†

Department of Chemical Engineering, University of Notre Dame, Notre Dame, IN 46556, U.S.A.

(*Received* 29 *March* 1993 *and in final form* 24 *November* 1993)

Abstract—A variational upper bound principle is used to derive equations for the Knudsen void gas thermal conductivity in three model fiber beds made up of randomly placed, freely overlapping, long right circular cylinders with their central axes mutually parallel, with each cylinder axis independently oriented in two dimensions or with each axis independently oriented in three dimensions. In order to establish the importance of dispersed solid shape and spatial distribution in predicting the low pressure gas conductivities in cryogenic insulation, the five fiber bed conductivities are compared with sphere bed and parallel plate Knudsen thermal conductivity equations for various values of the thermal accommodation coefficient.

INTRODUCTION

KNUDSEN transport occurs either at low pressures, or within the void space of a finely dispersed solid at normal pressures. Under these conditions the average distance between successive molecule–wall surface collisions is much smaller than the molecular mean free path, molecule–molecule collisions become unlikely and can be neglected. Gas heat conduction in cryogenic insulation, where the insulator space is usually evacuated and filled with a dispersed solid [1], is often in the transition or the Knudsen regime [2] and a knowledge of the Knudsen void gas thermal conductivity is needed for design considerations. Cryogenic insulation technology is important for natural gas upgrading and storage [3], liquid oxygen production, as well as the minimization of evaporation losses in space flight [4]. The low pressure Knudsen void gas conductivity k_{Kn} is commonly represented by an equation of the type

$$k_{Kn}\,(\mathrm{PS}) = C\delta\,[\alpha/(2-\alpha)], \tag{1a}$$

with

$$2C = k\psi\,(\gamma+1)/(\gamma-1) \tag{1b}$$

and

$$\psi = \bar{P}\bar{v}/(4k\bar{T}) \tag{1c}$$

In equations (1a)–(1c), k is the Boltzmann constant and γ is the heat capacity ratio C_p/C_v. The effusive driving force ψ, a constant across the cryogenic insulation, is customarily evaluated at an average pressure $\bar{P}$, average temperature $\bar{T}$, and associated mean thermal speed $\bar{v}$. The values [2] of the thermal accommodation coefficient α run from 0.0151 for He on clean tungsten at -190°C up to 1.0 for H_2 on glass at -170°C. Equation (1) is derived for parallel surfaces (PS model) [5, 6], where δ represents the plate spacing. Its application to other void–solid geometries is ad hoc, e.g. for cryogenic foam insulation δ is assigned to be the average cell size [4] and for dispersed solids δ is taken to be the average pore diameter [7] ($4\times$ void volume divided by the dispersed solid surface area). Any rigorous form of the Knudsen thermal conductivity, dominated by wall interactions, will be sensitive to the structure of the void space.

In a recent paper [8], a variational principle for the thermal conductivity of a void–solid suspension of arbitrary geometry with Knudsen gas conduction in the void space was formulated, and applied to a bed of randomly placed, freely overlapping solid spheres all of the same radius (OS model). If δ for the OS model is the average pore diameter ($4\times$ void volume divided by the dispersed solid surface area), the resulting variational equation for the Knudsen void gas conductivity from ref. [8] is

$$k_{Kn}\,(\mathrm{OS}) = C\delta\left[\frac{12}{9+4(1-\alpha)}\right]. \tag{2}$$

Equation (2) was shown to be the exact form of k_{Kn} at high void fraction for both $\alpha\to 0$ or $\alpha\to 1$, and agreed well with other approximate results [9] between these limits. The expression (2) also provided a rigorous upper bound on the Knudsen void gas conductivity for any lower void fraction. It has been demonstrated [8–11] that randomly overlapping spheres serve as an appropriate structure in which aspects of low pressure and radiation heat transport in random particulate dispersions can be displayed. That values of $k_{Kn}/(\delta C)$ from equation (2) always lie above those of equation (1) in Fig. 1 illustrates the influence of void–solid geometry on k_{Kn} and suggests in general the use of equation (1) will significantly underestimate the Knudsen gas thermal conductivity.

† Author to whom correspondence should be addressed.

NOMENCLATURE

a	fiber radius
A	defined in equation (6)
A_j	area in the j plane perpendicular to the fiber central axis ω_j.
A_{Rad}	defined in equation (3a)
C	defined in equation (1b)
C_{Rad}	defined in equation (3b)
$\mathrm{d}^2\mathbf{r}$	differential element of surface
$\mathrm{d}^3\mathbf{r}$, $\mathrm{d}^3\boldsymbol{\rho}$	differential elements of volume
E	surface energy efflux
$E(m)$	complete elliptic integral of the second kind
g	general function used in definition (15)
G_0	definite integral defined by equation (28)
G_1	definite integral defined by equation (29)
$\mathbf{i}$	unit vector across the slab from $x = 0$ to L
k	the Boltzmann constant
k_0, k_1, k_2, k_3	defined by equations (20)–(23)
k_{Kn}	Knudsen void gas conductivity
k_{eff}	effective conductivity
k_{s}	solid conductivity
$K(\mathbf{r}',\mathbf{r})\mathrm{d}^2\mathbf{r}$	differential view factor between two surface points
L	slab thickness
n_j	density of fiber centers of radius a per unit area in the j plane
P_j	probability that no circle center lies within an area A_j in the j plane
$\bar{P}$	average pressure
$\mathbf{r}$	location vector in either Σ or V_{s}
s	total void–solid interface area per unit slab volume
T	temperature
$\bar{T}$	average temperature
$\bar{v}$	mean thermal speed
V	total volume of the bed
V_{s}	total solid volume
V_ϕ	total void volume
x	coordinate across slab.

Greek symbols

α	fiber surface thermal accommodation coefficient
γ	heat capacity radio, $C_{\mathrm{p}}/C_{\mathrm{v}}$
γ_j, ξ_j	angular variables for cylinder orientation
δ	average pore diameter of fiber bed, $4\Phi/\mathrm{s}$
ε	fiber surface emissivity
$\boldsymbol{\eta}$	fiber surface unit normal
$\boldsymbol{\theta}$	temperature gradient defined by equation (8a)
λ	variational parameter
λ_{opt}	optimal value of λ
$\boldsymbol{\rho}$	displacement vector, $\mathbf{r}' - \mathbf{r}$
ρ_l	the projection of the vector $\boldsymbol{\rho}$ onto the l plane
σ	Stefan–Boltzmann constant
σ_j	total surface area of cylinders with orientation $\boldsymbol{\omega}_j$
Σ	surface area
Φ	void fraction
ψ	effusive driving force, $\bar{P}\bar{v}/4k\bar{T}$
$\boldsymbol{\omega}_j$	unit vector that gives the direction of the central axis of a cylinder.

Subscripts

eff	effective bed property
j	cylinders with central axis in the direction $\boldsymbol{\omega}_j$, and quantities in the corresponding j plane perpendicular to $\boldsymbol{\omega}_j$
Kn	Knudsen void gas
0, L	ends of the slab
Rad	radiation
s	solid
ϕ	void.

Superscript

*	trial functions for variational principle (5).

Operations

$\langle \ldots \rangle$	surface average defined by equation (15).

To further examine the structural sensitivity of k_{Kn} and treat another solid dispersion of importance in cryogenic technology [1], in this paper variational equations for the Knudsen conductivity will be derived for a number of model fiber beds made up of randomly placed, freely overlapping, long right circular cylinders with three different types of orientations—central axes mutually parallel (POC model); central axes oriented mutually at random, but with parallel vectors of rotation, i.e. parallel planes of rotation (PROC model); and central axes of each cylinder given an independent orientation, i.e. isotropic in three dimensions (IOC model). We will show that the values $k_{\mathrm{Kn}}/(\delta C)$ for the various principal axis directions within each of the random fibrous solid beds considered will always lie well above equation (1) and at or below the constant conductivity 2.47 for one-dimensional transport parallel down along the central axes of the POC model, i.e. $k_{\mathrm{Kn}}(\mathrm{POC}\|) = \delta C\pi^2/4$.

Barron [12] has pointed out that the Knudsen gas thermal transport equations are often of the same form as those of radiation transport. Wolf *et al.* [8] have shown that with the exchanges

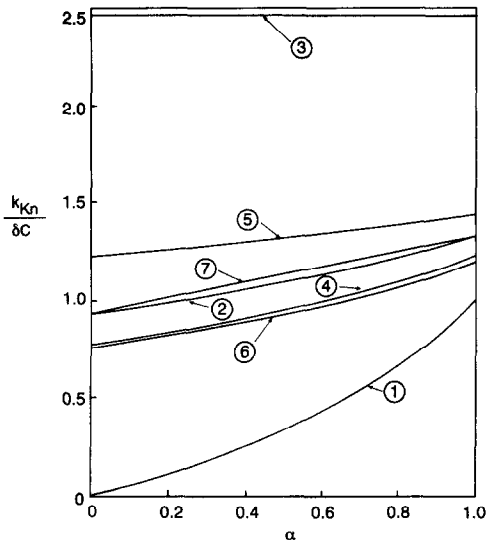

FIG. 1. Plots of the dimensionless Knudsen void gas thermal conductivities $k_{Kn}/(C\delta)$ vs thermal accommodation coefficient, α, for various dispersed solid geometries. ① Flux across the parallel surfaces model, equation (1). ② OS, three-dimensional isotropic bed of spheres, equation (2). ③ POC$\parallel$, flux down the fiber axes, equation (24). ④ POC$\perp$, flux perpendicular to the fiber axes, equation (26). ⑤ PROC$\parallel$, flux parallel to the planes of fiber rotation, equation (26). ⑥ PROC$\perp$, flux perpendicular to the planes of fiber rotation, equation (26). ⑦ IOC, three-dimensional isotropic fiber bed, equation (26).

$$A_{Rad} = -3\sigma\bar{T}^4, \tag{3a}$$

$$C_{Rad} = 4\sigma\bar{T}^3, \tag{3b}$$

and

$$\alpha = \varepsilon, \tag{3c}$$

where ε is the particle surface emissivity, $\bar{T}$ is the average of the edge temperatures and σ is the Stefan–Boltzmann constant, the k_{Kn} void gas variational principle and the resulting conductivity equations will give the equivalent void radiation conductivities k_{Rad}. As these random fiber bed models have already been used to address the mass transport [13,14], the k_{Rad} equations will be useful to model the accompanying radiation heat transport (process temperatures above 1200 K) within the ceramic fiber mat geometries (fiber diameters 10–150 microns) occurring [15, 16] during the chemical vapor intrusion processing of ceramic reinforced fiber composite materials.

VARIATIONAL PRINCIPLE

Consider a very large, thick slab of arbitrary void–solid geometry and total volume V extending from $x = 0$ to L. The total volume V is divided into two subregions, a region of solid volume V_s and void region V_ϕ. The interface between these two regions makes up the void–solid interface Σ. We assume that gas molecules in the void that strike the surface are either reflected diffusely or after energy equilibration are diffusely emitted from the surface according to the cosine law [17]. Any dependence of the energy accommodation coefficient α on the direction or energy of the incident or departing molecules is neglected.

Across the slab a steady temperature difference $T_O - T_L$ is maintained. A unit vector $\mathbf{i}$ points across the slab in the positive x-direction with a thermal gradient

$$\boldsymbol{\theta} = -(T_O - T_L)\mathbf{i}/L. \tag{4}$$

A knowledge of the energy $E(\mathbf{r})$ of the Knudsen gas molecules leaving a unit surface on Σ located at $\mathbf{r}$ per unit time both by emission and reflection, the local solid temperature $T(\mathbf{r})$ and the solid conductivity k_s is sufficient to calculate the effective thermal conductivity k_{eff} of the thick slab from

$$C\theta^2 k_{eff} \leqslant \frac{1}{2V}\int_\Sigma d^2\mathbf{r}\int_\Sigma d^2\mathbf{r}' K(\mathbf{r},\mathbf{r}')\,[E^*(\mathbf{r}') - E^*(\mathbf{r})]^2 + \frac{1}{V}\frac{\alpha}{1-\alpha}\int_\Sigma d^2\mathbf{r}[E^*(\mathbf{r}) - A - CT^*(\mathbf{r})]^2 + \frac{C}{V}\int_{V_s} d^3\mathbf{r}\, k_s[\nabla T^*(\mathbf{r})]^2. \tag{5}$$

The variational principle (5), derived in ref. [8] is listed in a form appropriate for radiation of Knudsen void gas thermal conduction, and the associated constants are given by either equations (3a)–(3c) for radiation, or by equations (1b)–(1c) with A for Knudsen conduction equal to zero,

$$A = 0 \text{ (Knudsen gas thermal conduction).} \tag{6}$$

The kernel function $K(\mathbf{r},\mathbf{r}')d^2\mathbf{r}$ is the differential view factor for particles diffusely leaving a unit surface at $\mathbf{r}'$ on Σ, and traveling directly to the surface element $d^2\mathbf{r}$ located at $\mathbf{r}$ also on Σ, whereas $d^3\mathbf{r}$ is a volume element located at a point $\mathbf{r}$ in V_s. Since we are assuming diffuse scattering at the surfaces, K is given by the cosine law,

$$K(\mathbf{r},\mathbf{r}') = K(\mathbf{r}',\mathbf{r}) \tag{7a}$$

$$= -[\boldsymbol{\eta}(\mathbf{r})\cdot\boldsymbol{\rho}]\,[\boldsymbol{\eta}(\mathbf{r}')\cdot\boldsymbol{\rho}]/(\pi\rho^4)$$

$$(\text{if } \mathbf{r} \text{ can see } \mathbf{r}') \tag{7b}$$

$$= 0 \text{ (otherwise).} \tag{7c}$$

$\boldsymbol{\eta}(\mathbf{r})$ and $\boldsymbol{\eta}(\mathbf{r}')$ are unit normals, respectively, at the points $\mathbf{r}$ and $\mathbf{r}'$ on Σ pointing into the void, and $\boldsymbol{\rho} = (\mathbf{r}' - \mathbf{r})$.

The asterisk superscript signifies trial forms of E and T, whose use in equation (5) produces a variational estimate and rigorous upper bound on k_{eff}. A simple selection for the trial temperature in the fiber beds is

$$T^*(\mathbf{r}) = T_0 + \boldsymbol{\theta}\cdot\mathbf{r}. \tag{8a}$$

The trial surface energy efflux equivalent [8] to equation (8a) is

$$E^*(\mathbf{r}) = A + CT^* + \lambda\boldsymbol{\theta}\cdot\boldsymbol{\eta}(\mathbf{r}), \tag{8b}$$

and λ is an adjustable parameter. Note that **i** in equation (4) and θ in equations (8a) and (8b) are in the direction of the applied thermal gradient which can be selected parallel or perpendicular to the various alignments of the cylinder axes.

RANDOMLY OVERLAPPING FIBER BEDS

To model a fibrous material, a large slab of total volume V and thickness L is cut from an infinite bed of very long right circular cylinders of radius a placed at random and allowed to freely overlap. A point lying within one or more cylinders is in the solid volume V_s, those points that lie outside the cylinders make up the void V_ϕ and points on a cylinder surface, not overlapped by any other cylinder, are the void–solid interface Σ. The internal structure of the cylinder bed depends on their orientations. In addition to the random placement, an orientation ω_j is assigned to each cylinder. The index j sums over a discrete or continuous set of orientations. A number of possibilities are of interest:

(a) all cylinders are given the same orientation with ω_j parallel to the **i** direction across the slab thickness (POC$\parallel$);

(b) all the cylinders are given the same orientation, but perpendicular to the **i** direction (POC$\perp$);

(c) each cylinder is given a random orientation in a plane with all vectors of rotation parallel to **i**, i.e. the fibers are oriented mutually at random perpendicular to the applied thermal gradient (PROC$\perp$);

(d) each cylinder is randomly oriented in a plane with the planes of rotation all parallel both to the vector **i** and to each other (PROC$\parallel$); and

(e) the cylinders are oriented isotropically, i.e. each cylinder axis is selected independently with any direction in three dimensions equally likely (IOC).

The statistics of a bed of cylinders has been discussed elsewhere [18,19], but, for the purpose of calculation of the variational integrals, it suffices to consider those cylinders with axial orientation vector ω_j and the j plane perpendicular to this direction [18]. Those cylinders with orientation ω_j appear as randomly overlapping circles of radius a in the j plane with centers randomly placed. The probability P_j that no circle center lies within an area A_j in the plane, can be written [19] in terms of the density n_j per unit area of circle centers in the j plane,

$$P_j = \exp(-n_j A_j). \tag{9}$$

The void fraction Φ can be interpreted as the probability that a randomly chosen point in the slab falls in the void, or the probability that in each given j plane no circle has its center within a distance a of the random point. Since the j planes are statistically independent and from P_j of equation (9)

$$\Phi = \exp\left(-\sum_j n_j \pi a^2\right) \tag{10}$$

where the summation is over any assigned fiber orientations of the model.

The surface area σ_j, overlapped or not, of those cylinders with orientation ω_j within a unit total volume of the slab is

$$\sigma_j = 2\pi a n_j. \tag{11}$$

From its product with the void fraction (10), we obtain the exposed portion s_j, the void–solid interface due to the ω_j cylinders

$$s_j = \sigma_j \Phi = 2\pi a n_j \Phi, \tag{12}$$

and the total void–solid interface area s per unit total slab volume

$$s = \sum_j s_j = \sum_j 2\pi a n_j \Phi. \tag{13}$$

For the case of a dispersed solid, δ is the average pore diameter and by its definition in equations (1) and (2)

$$\delta = 4\Phi/s = 2\left(\sum_j \pi a n_j\right)^{-1}. \tag{14}$$

When the trial functions (8a) and (8b) are substituted into the variational integrals (5), the integrand of the volume integral is a constant. In terms of the surface normals $\boldsymbol{\eta}$ ($\boldsymbol{\eta}'$) at $\mathbf{r}$ ($\mathbf{r}'$) and, $\boldsymbol{\rho} = \mathbf{r}' - \mathbf{r}$, the surface integrals are of the general form

$$\langle g(\boldsymbol{\rho},\boldsymbol{\eta},\boldsymbol{\eta}')\rangle = (sV)^{-1} \int_\Sigma d^2\mathbf{r} \int_\Sigma d^2\mathbf{r}' K(\mathbf{r},\mathbf{r}') g[\boldsymbol{\rho},\boldsymbol{\eta}(\mathbf{r}),\boldsymbol{\eta}(\mathbf{r}')]. \tag{15}$$

The function g in equation (15) can be $[\mathbf{i}\cdot\boldsymbol{\rho}\delta^{-1}]^2$, $[\mathbf{i}\cdot\boldsymbol{\rho}\delta^{-1}][\mathbf{i}\cdot(\boldsymbol{\eta}-\boldsymbol{\eta}')]$, $[\mathbf{i}\cdot(\boldsymbol{\eta}'-\boldsymbol{\eta})]^2$ or $[\mathbf{i}\cdot\boldsymbol{\eta}]^2$. The surface integrals also depend on $K(\mathbf{r},\mathbf{r}')$ given by equation (7), and, for any arbitrary set $\{\omega_j\}$ of cylinder orientations, the surface average (15) can be written

$$\langle g(\boldsymbol{\rho},\boldsymbol{\eta},\boldsymbol{\eta}')\rangle = -\frac{1}{\pi s}\sum_j\sum_k \frac{\sigma_j}{2\pi}\int_{\boldsymbol{\rho}\cdot\boldsymbol{\eta}_j\geq 0} d\theta_j \frac{\sigma_k}{2\pi}\int_{\boldsymbol{\rho}\cdot\boldsymbol{\eta}_k'\leq 0} \times d\theta_k' \int d^3\boldsymbol{\rho} \exp\sum_l [-2a\rho_l n_l - \pi a^2 n_l](\boldsymbol{\eta}_j\cdot\boldsymbol{\rho})(\boldsymbol{\eta}_k'\cdot\boldsymbol{\rho})\rho^{-4} g(\boldsymbol{\rho},\boldsymbol{\eta}_j,\boldsymbol{\eta}_k'). \tag{16}$$

This equation is derived in ref. [18] and appears as equation (21) in that publication. The integral (16) requires a sum without restriction over all possible j, k pairs as well as a separate sum over l. The projection ρ_l of the vector $\boldsymbol{\rho}$ onto the lth plane can be written

$$\rho_l = [\rho^2 - (\boldsymbol{\rho}\cdot\boldsymbol{\omega}_l)^2]^{1/2}. \tag{17}$$

The integrations over θ_j and θ_k' are performed over all possible angles 0–2π, respectively, in the j and k planes subject to the respective restrictions $\boldsymbol{\rho}\cdot\boldsymbol{\eta}_j \geq 0$ and $\boldsymbol{\rho}\cdot\boldsymbol{\eta}_k' \leq 0$. The $\boldsymbol{\rho}$ integration is done over the entire slab volume.

RESULTS AND DISCUSSION

Once the trial temperature (8a) and energy efflux (8b) are substituted into the variational principle (5), an optimal value of λ is selected,

$$\delta^{-1}\lambda_{\text{opt}} = -(1-\alpha)(k_0/k_3)^{1/2} \times\left[\frac{1}{2}+(k_1/k_0)-\frac{1}{2}k_2\right]^{1/2}(1+\alpha k_2)^{-1}. \quad (18)$$

We obtain from equations (5), (8a), (8b) and (18) the general variational form for the void–solid system effective conductivity, valid for an *arbitrary* dispersion geometry,

$$k_{\text{eff}} \leqslant \Phi\left[C\delta\left(\frac{k_0+\alpha k_1}{1+\alpha k_2}\right)\right]+(1-\Phi)k_s \quad (19)$$

The k integrals depend only on the bed microgeometry, and in terms of the surface averages (15)

$$\frac{k_0}{2} = \langle[\mathbf{i}\cdot\rho\delta^{-1}]^2\rangle - \frac{\langle[\mathbf{i}\cdot(\boldsymbol{\eta}'-\boldsymbol{\eta})]\,[\mathbf{i}\cdot\rho\delta^{-1}]\rangle^2}{\langle[\mathbf{i}\cdot(\boldsymbol{\eta}'-\boldsymbol{\eta})]^2\rangle}, \quad (20)$$

$$k_1 = \langle[\mathbf{i}\cdot\rho\delta^{-1}]^2\rangle(1+k_2)-k_0, \quad (21)$$

$$k_2 = \langle[\mathbf{i}\cdot(\boldsymbol{\eta}'-\boldsymbol{\eta})]^2\rangle^{-1}k_3-1, \quad (22)$$

with

$$k_3 = 2\langle[\mathbf{i}\cdot\boldsymbol{\eta}]^2\rangle \quad (23)$$

Note that a knowledge of the values of the four ks is sufficient to determine the four different bracketed surface averages in equations (20)–(23), and the k form (19) of the variational result for k_{eff} is convenient for the following discussion.

(a) POC$\|$. We consider first cylinders placed at random with axes mutually parallel and an applied gradient also parallel to the cylinder axes. For heat transfer down a very long channel with a constant cross-sectional shape, the temperature profile is both one-dimensional and linear. In addition $\mathbf{i}$ and the surface normal $\boldsymbol{\eta}$ are always perpendicular, i.e. $\mathbf{i}\cdot\boldsymbol{\eta}=0$, so that the bracketed averages (20)–(23) all vanish except $\langle[\mathbf{i}\cdot\rho\delta^{-1}]^2\rangle$, which from equation (16) equals $\pi^2/8$. The variational principle (19) then gives, not a bounding estimate, but the exact equality

$$k_{\text{eff}} = \Phi\,[C\delta\pi^2/4]+(1-\Phi)k_s. \quad (24)$$

The Knudsen thermal conduction and the solid conduction of equation (24) are in parallel,

$$k_{\text{eff}} = \Phi k_{\text{Kn}}+(1-\Phi)k_s, \quad (25)$$

the factors Φ and $(1-\Phi)$ are cross-sectional area fractions, respectively, of the void gas and solid, and the square bracketed term in equation (24) is the Knudsen gas thermal conductivity appropriate to compare with the parallel surface conductivity (1). Both the k_0 and the corresponding Knudsen thermal conductivity for POC$\|$ are given in the first row of Table 1. In the limit $\alpha\to 0$ the exact solution for the Knudsen thermal conductivity becomes mathematically equivalent to Knudsen mass diffusion in the same geometry. Knudsen particle diffusion by Monte Carlo simulations have been performed numerically by Tomadakes and Sotirchos [19] on all the cylinder bed structures in Table 1 and the simulation values of k_0 are given in the second column of Table 1. Simulation errors in some cases run as high as 2–5%, but the results are in excellent agreement.

For any of the following fiber bed models some general comments are useful for the interpretation of equation (19). In practice the solid fraction in cryogenic or refrigeration fibrous insulation [20] is very low (about 10%). At the same time for the disordered materials commonly used for insulation, such as glass, the conductivity monotonically drops to zero [21] in cryogenic temperature regions (below 200 K). A net effect of these circumstances is the solid conductivity term in equation (19) can often be neglected in cryogenic applications and thermal conduction occurs only in the void gas,

$$k_{\text{eff}} \leqslant \Phi\left[C\delta\left(\frac{k_0+\alpha k_1}{1+\alpha k_2}\right)\right] = \Phi k_{\text{Kn}}. \quad (26)$$

It is reasonable in equation (26) to drop the void cross section area factor Φ and identify the square bracketed term in equation (26) as the variational upper bound estimate of the cryogenic Knudsen void gas thermal conductivity to be compared with the parallel surface form (1). Note at high temperatures that the analogous condition of radiation equilibrium [8, 22] permits the same limit for the radiation k_{Rad} version (3a)–(3c) of equations (19) and (26). Also the use of the linear trial temperature (8a) in the solid volume term of the variational expression (third term in the right-hand side of equation (5)) gives a solid conductivity contribution in the parallel form (25). The other two integrals include the surface processes. It has been shown [8] that the trial energy efflux form (8b) can be derived from and is completely consistent with the linear temperature profile in the solid. When a random two-phase suspension consists of two Fourier solids, the upper bound variational principle with the linear trial temperature (8a) gives the parallel bound (25). It is interesting to note that the inequality equation (19) is also a parallel bound, if we take the square bracketed quantity in equation (19) to be the void Knudsen gas conductivity. Finally, note that a plot of k_{eff} versus k_s for fixed $\bar{T}$, $\bar{P}$, α and void–solid geometry will exhibit a single cross over from above to below the 45° diagonal line at the point $k_s = k_{\text{eff}} = k_{\text{Kn}}$. The application of inequality (19) at this point also affirms that the square bracketed term in equation (19) is a variational upper bound estimate of k_{Kn}. These k_{Kn} expressions for the following random fiber bed geometries are listed in the sixth column in Table 1 and are the Knudsen void gas conductivities appropriate to compare with the parallel surface conductivity (1).

Table 1. Knudsen void gas thermal conductivities for various cylinder distributions

	k_0 equation (20)	k_0 Monte Carlo [19]	k_1 equation (21)	k_2 equation (22)	k_3 equation (23)	k_{Kn} equation (19)
POC flux ∥ to fiber axes	$\frac{\pi^2}{4} = 2.467$	2.43	—	—	—	$\frac{C\delta\pi^2}{4}$
POC flux ⊥ to fiber axes	$\frac{2\pi^2}{16+\pi^2} = 0.7630$	0.763†	0	$\frac{-\pi^2}{16+\pi^2}$	1	$C\delta\left[\frac{2\pi^2}{16+\pi^2(1-\alpha)}\right]$
PROC flux ∥ to fiber axes	$\frac{8G_1}{8+G_1} = 1.221$	1.16†	0	$\frac{-G_1}{8+G_1}$	1	$C\delta\left[\frac{8\times 1.441}{8+1.441(1-\alpha)}\right]$
PROC flux ⊥ to fiber axes	$\frac{2G_0}{1+G_0} = 0.7488$	0.749†	0	$\frac{-G_0}{1+G_0}$	1	$C\delta\left[\frac{2\times 0.5985}{1+0.5985(1-\alpha)}\right]$
IOC	$\frac{12}{13} = 0.9231$	0.923†	$\frac{6}{13}$	$\frac{1}{26}$	1	$C\delta\left[\frac{12(2+\alpha)}{27-(1-\alpha)}\right]$

† Obtained from ref. [19] in limit $\phi \to 1$.

(b) POC⊥. In a second case parallel cylinders are placed at random and allowed to freely overlap, but the flux is perpendicular to the fiber axes. Note from column three that k_1 is zero and α only appears in the denominator of k_{Kn}. The k_0 simulation values listed in column two of Table 1, and marked with an asterisk, have been taken in the dilute cylinder bed limit. From its agreement with the k_0 simulation values, the anisotropic scattering ($\alpha \to 0$) form of k_{Kn} is exact for a dilute bed. For the opposite limit of no scattering ($\alpha \to 1$) since each fiber has a small radius ($a \ll L$) compared to the distance for thermal change, it is practically isothermal and emits isotropically. As the adjustable parameter coefficient λ_{opt} of the $\mathbf{i}\cdot\boldsymbol{\eta}$ term in equation (8b) vanishes for $\alpha \to 1$ from equation (18), the trial efflux also predicts isotropic emission and $C\delta\pi^2/8$ is the correct two-dimensional isotropic scattering thermal conductivity [23]. Between these limits k_{Kn} from Fig. 1 increases monotonically with α, and is at least a very good approximation [8]. As typical cryogenic fiber bed void fractions are 90% and as at these high porosities overlap is not dominant in our model, the POC⊥ form of k_{Kn} is a reasonable form for the Knudsen void gas conductivity in this particular cryogenic insulation fiber bed geometry.

(c) PROC. Each cylinder is randomly oriented in a plane and the cylinder planes of rotation are mutually parallel. The cylinders are allowed to overlap freely. In a third case the average flux is in a direction parallel to the planes, and in a fourth the flux is perpendicular across the planes of orientation. Assuming a homogeneous angular distribution of cylinder axes, we replace the n_j by $\beta d\gamma_j/\pi$ in equations (10), (13), (14), (16) and (17) and sum over j by an integration over γ_j form 0 to π,

$$n_j = \beta\, d\gamma_j/\pi \qquad 0 \leqslant \gamma_j \leqslant \pi. \tag{27}$$

The coefficient k_1 is zero in both flux directions leaving a monotonic increase of k_{Kn} with α from the denominator. The Knudsen void gas conductivity in column six of Table 1 can be obtained analytically in terms of a constant G_0 or G_1 in each case,

$$G_0 = \frac{\pi^2}{4}\int_0^1 \frac{v^2}{E(1-v^2)}\,dv = 0.5985\cdots(\text{PROC}\perp) \tag{28}$$

and

$$G_1 = \frac{\pi^2}{4}\int_0^1 \frac{(1-v^2)}{E(1-v^2)}\,dv = 1.441\cdots(\text{PROC}\parallel), \tag{29}$$

where $E(m)$ is the complete elliptic integral of the second kind [24]. The agreement of k_{Kn} for the anisotropic scattering limit ($\alpha \to 0$), with the simulation results [19], is obtained again in equivalent dilute beds. In the limit of no scattering ($\alpha \to 1$), the trial energy efflux (8b) $E^* = CT^*$ with the linear trial temperature (8a) is the exact choice for a dilute bed and the k_{Kn} are appropriate to compare with equation (1) to observe fiber bed structural effects in cryogenic insulations.

(d) IOC. For isotropic random orientation each of the freely overlapping, solid right circular cylinders is placed at random into the bed with an orientation independent of those of the other cylinders already present. For a homogeneous angular distribution of cylinder axes n_j is replaced by $\varepsilon \sin\xi_j\, d\xi_j\, d\gamma_j/(2\pi)$ and the sum over j by integrations over $d\gamma_j$ from 0 to 2π and $d\xi_j$ from 0 to $\pi/2$.

$$n_j = \varepsilon \sin\xi_j\, d\xi_j\, d\gamma_j/(2\pi) \quad 0 \leqslant \xi_j \leqslant \frac{\pi}{2}, 0 \leqslant \gamma_j \leqslant 2\pi. \tag{30}$$

The void Knudsen thermal conductivity in the anisotropic scattering limit ($\alpha \to 0$) gives the coefficient $\frac{12}{13}$.

This result, first proposed by Derjagiun [25], is known to be the exact solution for a dilute bed of spheres. The $\frac{12}{13}$ result agrees with the simulation value of k_0 and is the appropriate solution for a dilute three-dimensional isotropic bed of cylinders as well. In the isotropic scattering case ($\alpha \to 1$), the $\frac{4}{3}$ coefficient, a well-known exact result [22] for an isotropic dilute bed of particles, also provides the correct isotropic scattering solution of a dilute IOC cylinder bed. It is interesting to note that k_1 for this geometry does not vanish, and its 0.5 value is necessary to obtain the $\frac{4}{3}$ limit. Also for any other void fraction, the case of k_{Kn} in equation (19) or (25) gives an upper bound.

To demonstrate the effects of the different solid dispersions on the Knudsen void gas conductivity the dimensionless conductivity $k_{Kn}/(\delta C)$ is plotted versus the thermal accommodation coefficient in Fig. 1. Curves are numbered in the order they occur in the text and the curve numbers are circled. The parallel plate Knudsen conductivity, equation (1) and labeled ① on Fig. 1, provides a series lower bound on the $k_{Kn}/(\delta C)$ results we have derived. The Knudsen conductivity [8] for a bed of overlapping spheres equation (2), included for comparison as the granular structure, is labeled ②. The dimensionless thermal Knudsen flux down along the central axes of a bed of overlapping parallel cylinders, from Table 1 and labeled ③ on Fig. 1, in parallel transport with the solid, provides a horizontal line upper bound for the various geometries we have considered. The curve labeled ④, which provides the $k_{Kn}/(\delta C)$ values for the flux across the axes of the same parallel cylinders, always lies well below ③. For beds with each cylinder lying in parallel planes, but oriented mutually at random relative angles, the curves labeled ⑤ and ⑥ represent the flux parallel and perpendicular to the cylinder planes of rotation. That cylinders perpendicular to the flux block more effectively implies that ⑤ should lie above ⑥. From ③–⑤ effects of fiber rotation in the plane of a dilute fiber bed, where heat transfer is in that plane, is demonstrated. But from ④ and ⑥ the same fiber rotation for flux perpendicular to the fiber plane gives a small effect. The curve ⑦ for cylinder beds with three-dimensional isotropy, i.e. each cylinder oriented independently at random in three dimensions, has the same anisotropic and isotropic scattering limits as the three-dimensional isotropic sphere bed ②. However as k_1 is 0.5 and k_2 is small at 0.038, the three-dimensional isotropic cylinder bed curve is nearly a straight line, whence the sphere bed equation (2) has a positive curvature between the limits.

This study is focused on fiber and spherical dispersed solid beds and the most useful model curves of $k_{Kn}/(\delta C)$ seem to lie between 0.5 and 1.5 on Fig. 1. For the higher void fractions often met in practice ($\Phi \sim 0.9$), the results on Table 1 and Fig. 1 should be predictive for cryogenic insulation systems. An overview of Fig. 1 in the anisotropic limit ($\alpha \to 0$) shows a real diversity in the actual Knudsen conductivities with shape, ①–④, and arrangement, ③–⑦, but even for the isotropic case ($\alpha \to 1$) significant effects of dispersed solid geometry remain in cryogenic beds. Unfortunately the parallel surface equation (1) seriously underestimates k_{Kn} for any α, but particularly at lower α estimates from equation (1) will be very misleading.

SUMMARY AND CONCLUSIONS

One purpose of this paper was to derive various forms of the Knudsen void gas thermal conductivity, in order to study the importance of solid shape and spatial distribution in model fiber beds similar to those found in some dispersed solid cryogenic insulations. In Fig. 1 the *a priori*, variational Knudsen conductivities of the various solid fiber dispersions are compared, along with those of a bed of randomly overlapping spheres and the parallel plate model, as plots of $k_{Kn}(\delta C)^{-1}$ versus the thermal accommodation coefficient.

1. The POC‖ exact conductivity for parallel conduction provided an upper bound for the dispersions considered, while the parallel plate series equation (1) gave a lower bound.
2. The state of the art [1], Knudsen void gas thermal conductivity equations (1a)–(1c) for $k_{Kn}(\delta C)^{-1}$, where δ is either the parallel plate separation (multilayer insulation), the average pore diameter (fiber or powder insulant) or cell diameter (foams), suggest the form $\alpha(2-\alpha)^{-1}$ independent of insulant structure. Figure 1 demonstrates $k_{Kn}(\delta C)^{-1}$ for model cryogenic insulations lies in the range 0.5–1.5 and a sensitivity to insulant structure exists. Further the parallel plate predictions are too low.
3. The parallel plate equations (1a)–(1c) predict a very strong variation of $k_{Kn}(\delta C)^{-1}$ $[=\alpha(2-\alpha)^{-1}]$ with thermal accommodation α. Figure 1 shows that the factor $\alpha(2-\alpha)^{-1}$ overestimates the decrease in $k_{Kn}(\delta C)^{-1}$ with decreasing α.
4. The equation

$$k_{Kn}(\delta C)^{-1} = \frac{k_0 + \alpha k_1}{1 + \alpha k_2}$$

should assist in a systematic inclusion of insulant packing in thermal design. The equations for k_{Kn} given in Table 1 also apply to high temperature radiation heat transfer in the manufacture of fiber reinforced ceramics [8, 13, 16].

Acknowledgement—Acknowledgment is made to the donors of the Petroleum Research Fund, administered by the American Chemical Society, for support of this research.

REFERENCES

1. M. G. Kagner, *Thermal Insulation in Cryogenic Engineering*. IPST Press, Jerusalem (1969).
2. G. S. Springer, Heat transfer in rarefied gases, *Advan. Heat Transfer* **7**, 163–218 (1971).
3. B. A. Hands, A survey of cryogenic engineering. In *Cryo-*

genic Engineering (Edited by B. A. Hands), pp. 1–37. Academic Press, New York (1986).
4. R. L. Pleasant, Heat transfer through liquid hydrogen tank insulation on shuttle/centaur G-prime. In *Cryogenic Properties, Processes and Applications* (Edited by A. J. Kidnay, M. J. Hiza, T. N. K. Frederking, P. J. Kerney and L. A. Wenzel), Vol. 82, pp. 75–80. A.I.Ch.E. Symposium Series (1986).
5. S. Masamune and J. M. Smith, Thermal conductivity of beds of spherical particles, *I&EC Fund.* **2,** 136–145 (1963).
6. E. H. Kennard, *Kinetic Theory of Gases*, p. 314. McGraw-Hill, New York (1938).
7. G. R. Cunnington, Jr. and C. L. Tien, Heat transfer in microsphere insulation in the presence of a gas, *15th International Conference on Thermal Conductivity*, Ottawa, pp. 325–333. Plenum Press (1977).
8. J. R. Wolf, J. W. C. Tseng and W. Strieder, Radiation conductivity for a random void–solid medium with diffusely reflecting surfaces, *Int. J. Heat Mass Transfer* **33,** 725–734 (1990).
9. A. Dayan and C. L. Tien, Heat transfer in a gray planar medium with linear anisotropic scattering, *Trans ASME J. Heat Transfer* **97,** 391–396 (1975).
10. Y. Xia and W. Strieder, Complementary upper and lower truncated sum, multiple scattering bounds on the effective emissivity, *Int. J. Heat Mass Transfer* **37,** 443–450 (1994).
11. Y. Xia and W. Strieder, Variational calculation of the effective emissivity of a random bed, *Int. J. Heat Mass Transfer* **37,** 451–460 (1994).
12. R. F. Barron, *Cryogenic Systems*. Clarendon Press, Oxford University (1985).
13. M. M. Tomadakis and S. V. Sotirchos, Effect of fiber orientation and overlapping on Knudsen, transition, and ordinary regime diffusion in fibrous substrates. In *Chemical Vapor Deposition of Refractory Metals and Ceramics* (Edited by T. M. Besmann and B. M. Gallois), Vol. II, pp. 221–226. MRS, Pittsburgh (1992).
14. M. M. Tomadakis and S. V. Sotirchos, Transport properties of random arrays of freely overlapping cylinders with various orientation distributions, *J. Chem. Phys.* **98,** 616–626 (1993).
15. E. Fitzer and R. Gadow, Fiber reinforced silicon carbide, *Ceram. Bull.* **65,** 326–335 (1986).
16. G. R. Hopkins and J. Chin, SiC matrix/SiC fiber composite: a high heat flux, low activation structural material, *J. Nucl. Mater.* **141–143,** 148–151 (1986).
17. V. P. Shidlovskiy, *Introduction to the Dynamics of Rarefied Gases*. Elseveir, New York (1967).
18. T. Faley and W. Strieder, The effect of fiber orientation on Kundsen permeabilities, *J. Chem. Phys.* **89,** 6936–6940 (1988).
19. M. M. Tomadakis and S. V. Sortrichos, Effective Knudsen diffusivities in structures of randomly overlapping fibers, *A.I.Ch.E. Jl* **37,** 74–86 (1991).
20. C. L. Tien and A. J. Stretton, Heat transfer in low temperature insulation. In *Heat and Mass Transfer in Refrigeration and Cryogenics* (Edited by J. Bougard and N. H. Afgan), pp. 1–13. Hemisphere, New York (1987).
21. K. D. Timmerhaus and T. M. Flynn, *Cryogenic Process Engineering*. Plenum Press, New York (1989).
22. R. Siegel and J. R. Howell, *Thermal Radiation Heat Transfer*. McGraw-Hill, New York (1992).
23. A. Devera and W. Strieder, Upper and lower bounds on the thermal conductivity of a random two-phase material, *J. Phys. Chem.* **81,** 1783–1790 (1977).
24. M. Abramowitz and I. A. Stegun, *Handbook of Mathematical Functions*. National Bureau of Standards, Washington, DC (1964).
25. B. Derjaguin, Measurement of the specific surface of porous and dispersed bodies by their resistance to the flow of rarefied gases, *Compt. Rend. Acad. Sci. URSS* **53,** 623–626 (1946).